DOI 10.1515/aot-2012-0061 — Adv. Opt. Techn. 2013; 2(3): 257–268

Research Article

Hao Zhang, Sebastian Scheiding, Lei Li, Andreas Gebhardt, Stefan Risse, Ramona Eberhardt, Andreas Tünnermann and Allen Y. Yi*

Manufacturing of a precision 3D microlens array on a steep curved substrate by injection molding process

Abstract: In this study, a high volume low cost manufacturing method for microoptical microlens arrays on steep curved substrates using a microinjection molding technique was investigated. The design of the individual lenslets was performed using ZEMAX. This 3D microlens array in this study contains 1219 microlenses that are evenly distributed on its concave surface with a high fill factor. The overall field of view of this microlens array on curved substrates is more than 104°. To complete the manufacturing process, first the mold inserts were machined using a voice coil based fast tool servo technique, then the 3D microlens arrays were injection molded. The injection molding process parameters were evaluated using both experiments and numerical simulation for best molding results. In addition, both geometrical errors and optical performance tests showed that the molded polymer microlens arrays can be used in wide angle imaging applications. This study demonstrated that this combined process is capable of fabricating high precision microlens arrays at steep curved substrates at low cost. The microlens arrays created in this study have broad applications in optical, medical and biomedical domains. The success of this study provided a feasible solution for mass production of 3D microlens arrays on arbitrary substrates.

Keywords: 3D microlens array; 3D micromachining; microinjection molding.

OCIS codes: 220.0220; 120.4610; 130.3990; 160.5470; 220.4000; 230.3990.

***Corresponding author: Allen Y. Yi,** Department of Integrated Systems Engineering, The Ohio State University, 210 Baker Systems, 1971 Neil Ave, Columbus, OH 43210, USA, e-mail: yi.71@osu.edu

Hao Zhang and Lei Li: Department of Integrated Systems Engineering, The Ohio State University, 210 Baker Systems, 1971 Neil Ave, Columbus, OH 43210, USA

Sebastian Scheiding and Andreas Tünnermann: Fraunhofer Institute for Applied Optics and Precision Engineering, Albert-Einstein-Strasse 7, 07745 Jena, Germany; Friedrich Schiller University Jena, Institute of Applied Physics, Jena, Germany

Andreas Gebhardt, Stefan Risse and Ramona Eberhardt: Fraunhofer Institute for Applied Optics and Precision Engineering, Albert-Einstein-Strasse 7, 07745 Jena, Germany

1 Introduction

Accurate microstructures are becoming increasingly important for their wide applications in optical, electronic, biomedical and medical domains [1–4]. Precision microstructures, such as microlens arrays, have been fabricated using different methods [5–9]. Most of these methods were successfully used to produce uniform micro features with controlled surface profiles. However, these processes were mainly used to create features on planar substrates.

For 3D micromachining, photolithography based methods were developed, including, but not limited to, multilayer exposure [10], gray-scale lithography [11] and micro loading effect in reactive ion etching [12]. However, these methods tend to be technically complex and often require expensive facilities. Besides, most of these methods approximate 3D microstructures by performing multilayer 2D exposure and repeated alignment. These methods are more precisely 2.5D micromachining, restricting their applications. In addition to photolithography based methods, processes based on substrate reshaping was also attempted by some researchers [13–15], which was realized by fabricating microstructures on 2D flexible substrates and then transferring them to a non-planar substrate. This method changed the shape of the substrate, therefore has limitation in substrate material and pattern feature selection making it less suitable for

mass production. Except these, 3D microlens arrays were also successfully developed by another method [16, 17], in which the polymethylmethacrylate (PMMA) substrates were indented by designed indenters and afterwards immersed into ethanol to form the designed shapes.

The hot compression molding method was also utilized to create simple micro features [18, 19]. This method is preferred for industrial scale mass production, because of its low cost and high efficiency. However, 3D microstructures such as the 3D microlens arrays cannot be easily fabricated using this method because of the difficulties involved in mold making. In recent years, efforts have been made to apply the slow tool servo (STS) ultraprecision diamond machining technique to creating 3D microstructures [20–22]. However, STS is usually the primary choice for manufacturing freeform optical surfaces with large deviations. With the development of the fast tool servo (FTS) technique aimed for fabrication of small peak-to-valley micro features [23, 24], it is possible to fabricate molds with precise 3D microstructure arrays with high accuracy and precision at high production rates. Thereby, a combination of precision mold fabrication and a high efficient microinjection molding process can be a possible solution to manufacturing microstructure arrays with high optical quality in high volume.

In this study, the 3D microlens arrays on curved substrates were fabricated based on the combination of FTS and the microinjection molding technique. The aim of this design was to develop a device with a wide field of view (FOV), a high fill factor and compact size. The main objective of this study was to investigate the 3D micromachining capability of microinjection molding using mold inserts that were machined by a voice coil FTS. The process parameters were carefully considered using computer simulation and proper conditions were identified to fabricate the microlens arrays on steep curved substrates of high optical quality. To evaluate fabrication quality, the 3D microlens arrays were measured for both geometrical accuracy and optical performance with a focus on large FOV imaging applications. The efforts in this study can be utilized in achieving microlens arrays of high optical quality at very low manufacturing cost.

2 3D Microlens array design

Compared with 2D microlens arrays, microlens arrays on curved substrates have a much wider FOV. In an earlier publication [25], a microlens array on curved substrates based on the projection method has been successfully developed. However, the resulting patterns have a relatively low fill factor. In this study, the strategy of the design is to pursue a wide FOV and a high fill factor while maintaining a compact size. This 3D microlens array can be applied to 3D projection generating a complex micro feature array with high fill factor on curved substrates. In addition, the 3D microlens array can also be developed into optical devices needed for integrated imaging, solar energy concentration, and 3D motion detection.

The layout of the 3D microlens array is shown in Figure 1. At the bottom of the spherical substrate 1219 lenslets are evenly distributed and can be divided into 21 layers. For the spherical substrate, the radius of its top surface R_T is 12.5000 mm, and the radius of its bottom surface R_B is 11.0111 mm. The cross-section of the 3D microlens array is displayed in Figure 1A. Along the x-axis, there are 21 lenslets namely from n_1 to n_{21}, which represent layer 1 to layer 21. At each layer, the lenslets are generated by rotating around the z-axis, as shown in Figure 1B. Details of the lenslet

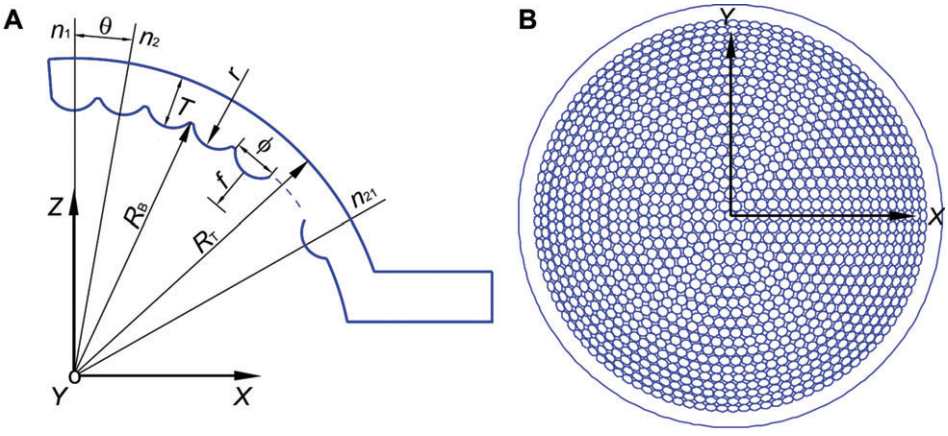

Figure 1 Design of the 3D microlens array on curved base. (A) Cross-sectional view, (B) top view.

Table 1 Lenslet layout.

Layer	Layer normal direction (°)	Lens number	Layer	Layer normal direction (°)	Lens number	Layer	Layer normal direction (°)	Lens number
1	0	1	2	2.6027	6	3	5.2054	12
4	7.8081	18	5	10.4107	24	6	13.0134	31
7	15.6161	37	8	18.2188	43	9	20.8215	49
10	23.4242	54	11	26.0269	60	12	28.6295	66
13	31.2322	71	14	33.8349	76	15	36.4376	82
16	39.0403	87	17	41.6430	91	18	44.2457	96
19	46.8483	100	20	49.4510	105	21	52.0537	110

layout are listed in Table 1. The information of the normal direction of each layer measured from the *z*-axis is also listed in Table 1. The included angle from layer 21 to the *z*-axis is 52.0537°, giving the overall FOV of the 3D microlens array to be more than $52.0537 \times 2 = 104.114°$. The individual lenslets were designed and optimized using ZEMAX. As indicated in Figure 1A, the diameter of the aperture of each individual lenslet φ is 0.5 mm, and the radius of the bottom surface *r* is 3.80828 mm. The thickness of each individual lenslet *T* is 1.5 mm. The back focal length is 5.8 mm, resulting in an *f*/# of 11.6. A larger *f*/# helps reduce aberrations and therefore improves imaging quality.

The angular resolution of individual lenslet is approximately 0.08° according to the Rayleigh criterion shown in Eq. (1).

$$\sin\theta = 1.22\frac{\lambda}{\phi} \tag{1}$$

where θ is the angular resolution in radian, λ is the wavelength of light. The angular resolution is larger compared to a macro size individual lens, because the 3D microlens array sacrifices the angular resolution of individual lenslets to improve its overall FOV, which is very similar to the strategy of compound eyes in nature. An image of wide FOV by individual lenslets can be achieved by adding an aperture array behind the 3D microlens array to prevent crosstalk among adjacent lenslets. Three different incident angles: 0°, 5°, and 10° were employed to demonstrate the simulated angular performance of the individual lenslets. A diagram of the spots for the incident rays is shown in Figure 2A. The sizes of the spots are listed in Table 2, indicating that off-axis aberrations are reduced, even for the 10° incident beam.

The optical performance of the individual lenslet was simulated using ZEMAX (Radiant Zemax Corporate Offices & Research Center, Redmond, WA, USA), based on the F, D, C visible wavelengths (486.1327, 587.5618, and 656.2725 nm). The cross-section of the point spread function (PSF) is shown in Figure 2B. Two diffraction rings can be seen clearly with the diameter of the first dark ring at 7.0325 μm with approximately 86% of the energy inside the first ring. Figure 2C displays the optical path difference (OPD) of the lenslet. The maximum values for the F, D, C wavelengths are 0.0862, -0.0315, and -0.0683 waves, respectively. The modulation transfer function (MTF) is displayed in Figure 2D. The spatial frequency cut-off values for the three wavelengths are 170.636, 139.491, and 124.237 Lp/mm.

3 Injection molding fabrication

The insert for injection molding, as shown in Figure 3A, was fabricated using a voice coil based FTS technique on a Nanotech 450 UPL machine (Moore Nanotechnology Systems, LLC, Swanzey, NH, USA) (www.nanotechsys.com). The finished insert has a surface roughness that is less than 4 nm. The overall form error of this freeform surface deviates below ±3 μm from the nominal value. The customized program and the results of the diamond turned microoptical lens arrays on a steep curved substrate by use of a voice coil FTS process were summarized by Scheiding et al. earlier [24]. The Sodick microinjection molding machine (Sodick Plustech Co. Ltd., Tsuzuki-ku, Yokohama, Kanagawa, Japan) used in this study can deliver a maximum clamping force of 30 ton and a maximum injection velocity of 250 mm/s [26, 27]. This machine is also capable of injecting a very small amount of polymer (<1 g) with three times the packaging pressure of a conventional injection molding machine and therefore can transfer the detailed micro features from the mold inserts to the polymer components. A common optical grade material, PMMA (GE Polymerland Inc., code named Plexi-glas1 V825–100), was used to fabricate the 3D microlens arrays. Important material properties of the polymer used for this study are listed in Table 3.

3.1 Microinjection molding simulation

The microinjection molding fabrication process was simulated using CAE software Moldex3D (CoreTech System Co., Ltd. Chupei City, Hsinchu County, Taiwan) (www.moldex3d.com/en/) to study the surface deviation due to

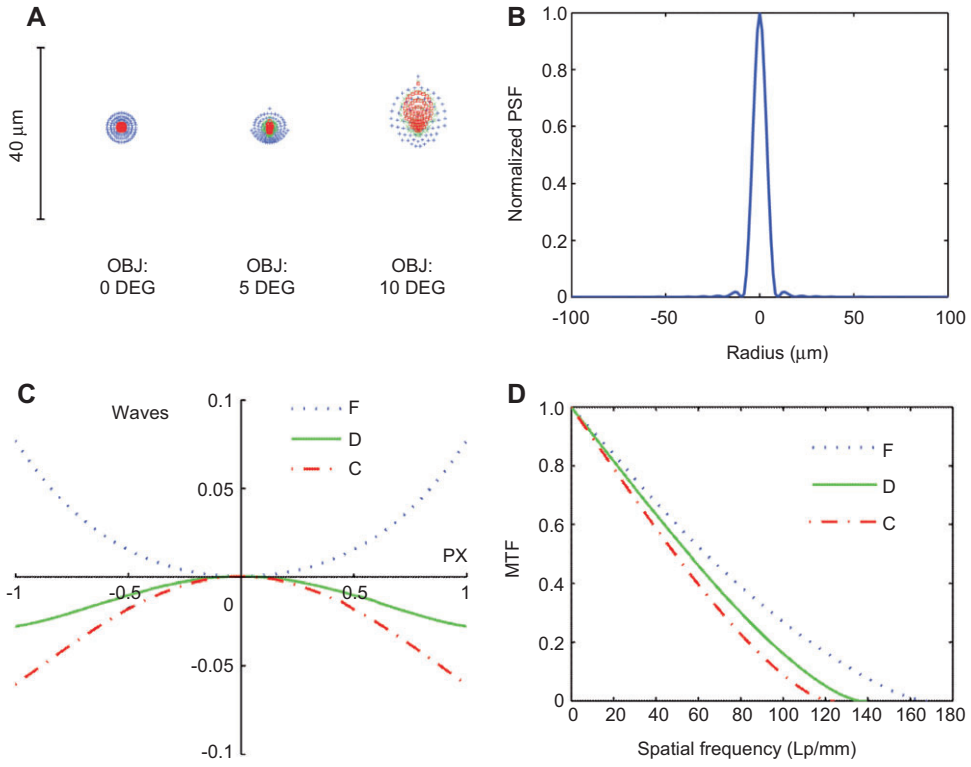

Figure 2 Optical performance of the individual lenslet, based on F, D, C wavelengths. (A) Diagram of the spots, (B) PSF, (C) OPD, (D) MTF.

Table 2 Angular performance of the individual lenslet.

Incident angle	RMS radius (µm)	Geometrical radius (µm)
0°	1.498	3.464
5°	2.040	6.409
10°	4.486	10.918

thermal shrinkage of the 3D microlens array. A solid model was first built in Solidworks and meshed using Hypermesh. The micro features at the bottom surface were removed from the model to simplify the numerical simulation. The PMMA material data employed in the experiments was imported from the Moldex3D database. The parameters setting of the microinjection molding process were based on previous experience. In microinjection molding of polymer optics, a higher melt temperature was preferred because the polymer viscosity is further reduced and therefore the melt flow can be improved in the filling stage [26–28]. Furthermore, the PMMA melt with a higher temperature needs more time to cool down and therefore allows more effective

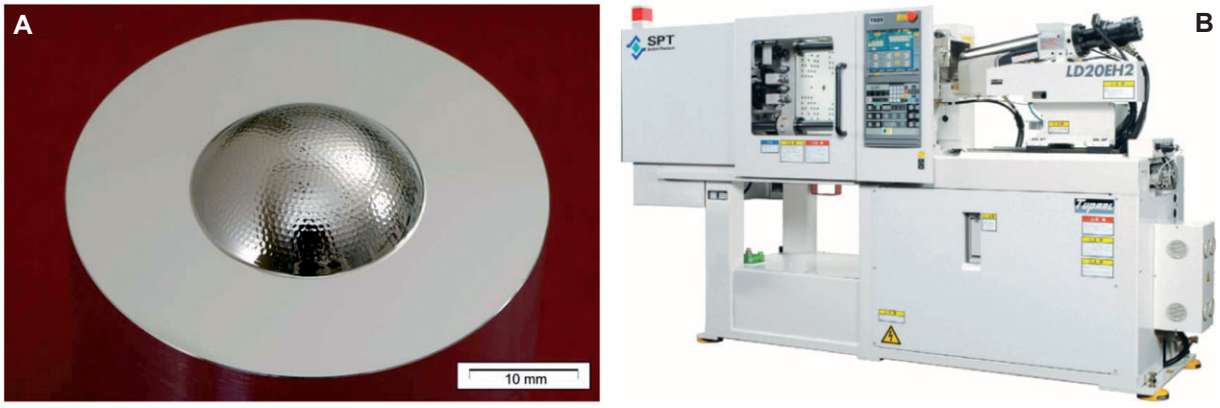

Figure 3 (A) Finished mold insert. (B) Sodick microinjection molding machine.

Table 3 Properties of Plexi-glas1 V825–100.

Material properties	Value
Glass transition temperature, T_g	101°C
Solid density, ρ	1.172 g/cm^3
Refractive index, n	1.4890
Luminous transmittance	92%
Polymer melt flow rate (230°C/3.8 kg)	3.7 g/10 min
Water absorption (24 h immersion)	0.3% of resin weight

packing. A higher injection speed can help the PMMA melt flow into the cavity quickly to avoid rapid cooling in the delivery system. Although higher packing pressure and longer packing time lead to more material flowing into the cavity [27], excessive packing pressure may cause uneven distribution of density, resulting in variations in refraction index. Moreover, if the packing time is too long the gate will be frozen thus preventing material from flowing into the cavity. In this study, the optimized fabrication conditions were studied using numerical simulation as summarized in Table 4. After microinjection molding was completed, both simulation and experimental results are plotted in Figure 6 in Section 4.2 for further study.

Table 4 Processing parameters used in this study.

Parameters	Value
A: Barrel temperature	260°C
B: Packing pressure	100 MPa
C: Packing time	8 s
D: Injection speed	200 mm/s
E: Mold temperature	70°C
F: Cooling time	12 s
G: Injection pressure	150 MPa
H: Velocity/pressure switch	90%

3.2 Microinjection molding process

The microinjection molding process was performed using the same conditions identified in numerical simulation. The process involves four steps: namely, preparation, filling, packing, and cooling. First, PMMA resins were dried in an oven at 88°C for 4 h to remove moisture and other contaminations in the material. PMMA pellets were then heated to 260°C, a temperature that is much higher than glass transition temperature (T_g) of PMMA to liquefy polymer resins. A proper shot size was set to ensure enough material flow into the mold cavity and to control dimensional accuracy. The injection velocity was identified as 200 mm/s, and the injection pressure was 150 MPa. Packing is a very important step to reduce the volume shrinkage of the workpiece. In this study, packing pressure was 100 MPa and packing time was 8 s. To reduce thermal stresses caused by fast cooling, mold temperature was controlled by a water-based Matsui MC-25 mold temperature controller. According to computer simulation, cooling at temperature of 70°C was adopted. Cooling time was set at 12 s to ensure that the workpiece can be released. When cooling completed, a microlens array on a curved substrate was manufactured.

4 Geometrical errors characterization

A finished 3D microlens array is shown in Figure 4A. Figure 4B shows a close-up view using a scanning electron microscope (SEM). To further study the geometrical errors introduced during the fabrication process, the surface roughness, form errors, and surface deviations were evaluated.

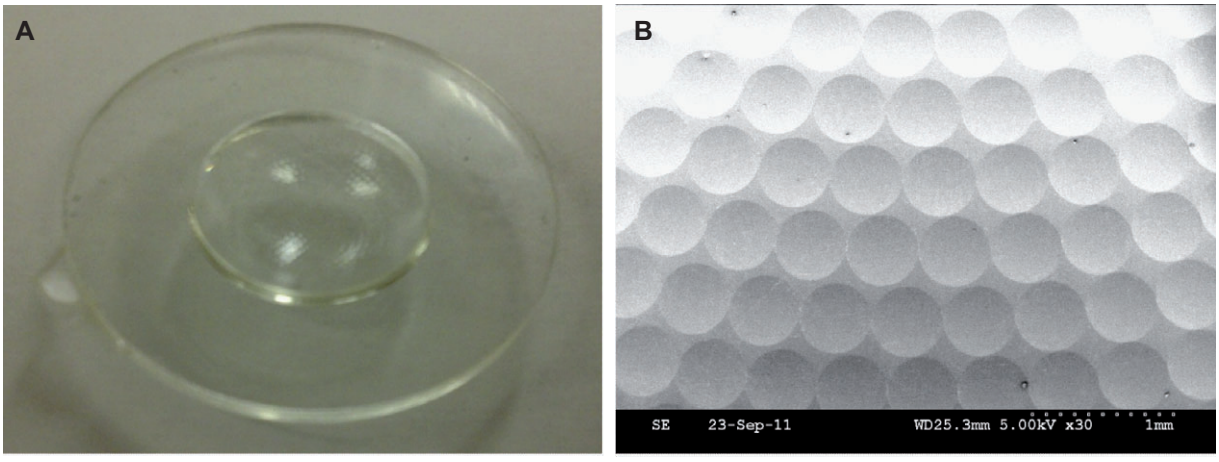

Figure 4 (A) A molded microlens array. (B) SEM of the molded microlens array.

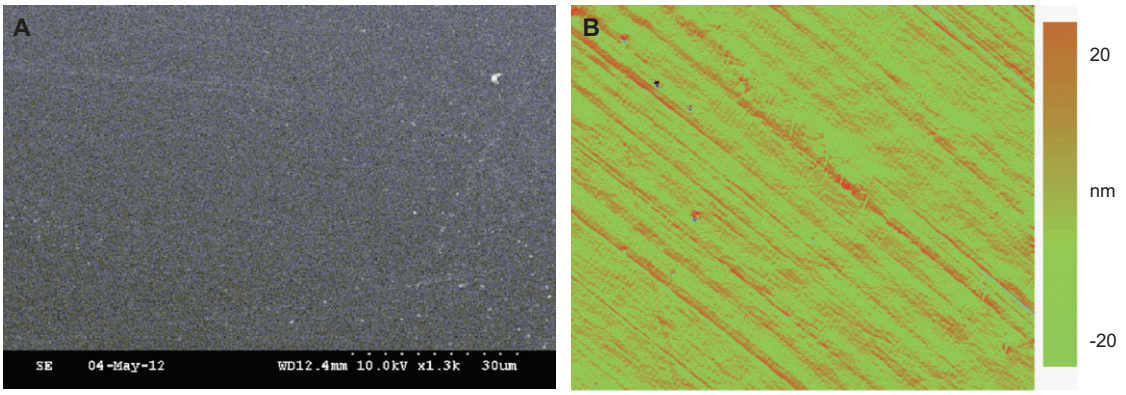

Figure 5 (A) SEM photo showing close-up view of a lenslet surface. (B) Surface roughness of the PMMA surface in a field of 126 μm × 96 μm inside a microlens using the Wyko interferometer.

4.1 Micro surface roughness

First, an SEM image was employed to present the close-up view of the lenslet surface, as shown in Figure 5A. To measure the surface roughness, a white light interferometer (Wyko NT9100, Bruker AXS Inc., Madison, WI, USA) was utilized, as shown in Figure 5B. This measurement was performed in a field of 126 μm × 96 μm, with a best-fit spherical surface removed from the measurement. To form an optical surface, the roughness should be 10 to 20 times smaller than the light wavelengths [26]. For this measurement, the arithmetical mean roughness (R_a) is 4.77 nm, the root mean square roughness (R_q) is 6.31 nm, and the total height of the roughness (R_t) is 234.89 nm. The measured root mean square roughness is close to that of the mold insert, which is 3.9 nm [24], demonstrating a smooth surface.

4.2 Form error

The overall shape deviation of the 3D microlens array was measured using a tactile 3D profilometer (UA3P-5, Panasonic). First, the profilometer was utilized to scan the surface of the microlens array with a contact probe that has a tip of 2 μm radius. The non-uniform point cloud data were exported from the Panasonic proprietary analysis software, which is not capable of analyzing the entire arrays of micro lenses on curved surfaces and interpolated to fit a uniform homogeneous polar mesh. Subsequently, the overall shape deviation is divided into two parts: rotationally symmetric error and freeform error to obtain the exact information for error compensation. The rotationally symmetric error can be corrected in the microinjection molding process or as part of iterative steps in mold manufacturing. The freeform error shows the asymmetric deformations of the parts and can be partially corrected by changing the mold design and by adjusting injection molding parameters. As shown in Figure 6B,C, the peak-to-valley (PV) value of the overall shape error is 22 μm, the PV value of the rotationally symmetric error is 17 μm, and the PV value of the freeform error is 12 μm. The simulation result for the overall shape error is shown in Figure 6A, and the PV value of the simulated result is 23 μm, and shows a little difference with the overall shape error. The difference may be caused by many reasons such as the math model associated with the calculation, the material property in the database, and the actual operational machine status. Besides, the individual 1219 microlenses were removed from the substrate to simplify the simulation process. Although the difference exists, the simulated shape error predicted the measured overall shape error well, validating the selected process parameter combination.

The amount of shape error is largely due to volume shrinkage, which occurred during cooling. Because the cooling rate across the lens cavity was different, it resulted in uneven temperature gradient along the radial direction. The PMMA material was cooled faster at the edge and thus has less time to relax resulting in a larger volume. Overall, the molded lenses are thinner at the center and become increasingly thicker in the radial direction. Because material relaxation is both temperature- and temperature gradient-dependent, the overall shrinkage is the result of a strong nonlinear process. This deviation, however, can be compensated for using multiple iterations with the finite element method based numerical simulation [29, 30], providing a practical solution for manufacturing high precision 3D polymer microlenses at low cost.

4.3 Surface deviation

The surface deviation of the individual lenslet from the designed spherical surface was measured using the Wyko

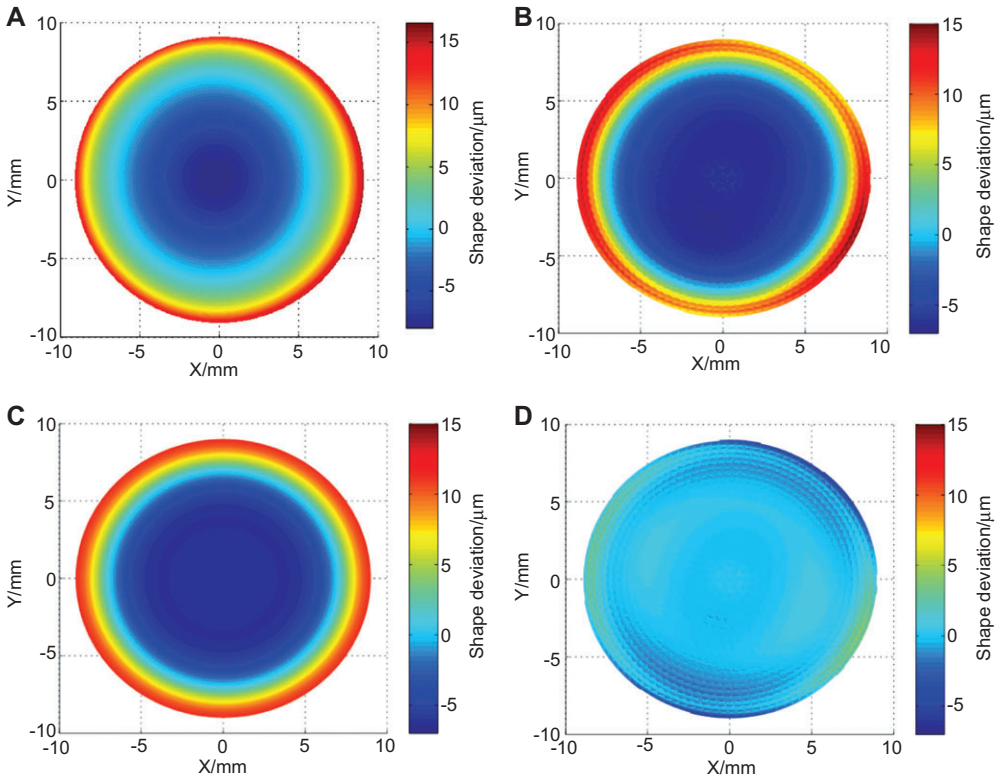

Figure 6 Shape deviation from the nominal spherical surface. (A) Simulated overall shape deformation using Moldex3D. (B) Measured overall shape deformation using UA3P-5. (C) Rotationally symmetric error. (D) Freeform error.

white light interferometer. After being subtracted by the design spherical surface of 3.80828 mm radius, a section of the deviation is displayed in Figure 7A. Figure 7B shows a cross-section of the deviation map, as indicated by the red arrow in Figure 7A. From the results, the deviation is shown to have increased slightly from the center to the edge of the lenslet. At the center, the average deviation is -20 nm. At the edge, the maximum deviation appears but still within 250 nm. Compared with the overall lens sag height which is 8.215 µm, the low surface deviation indicates a highly spherical surface.

5 Optical performance characterization

To evaluate fabrication quality, optical performance of individual lenslets was measured using a home-built metrology system consisting of a Mach-Zehnder interferometer (MZI) and a Twyman-Green interferometer (TGI) using a He-Ne laser (632.8 nm), as shown in Figure 8. There are three optical switches in this system to select the type of interferometer. When switch 1 (S1) is turned off,

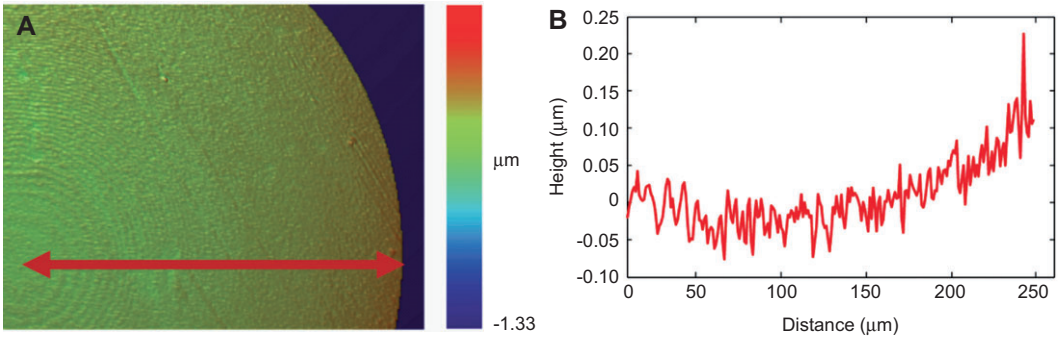

Figure 7 Surface deviation from the design spherical surface. (This measurement was performed inside an individual microlens, by using the Wyko white light interferometer.)

switch 2 (S2) and switch 3 (S3) are on, the system is an MZI, otherwise the system is a TGI.

The focal length was measured in several steps. First, in the TGI mode, the 3D microlens array was moved along the *X* direction until the focal point arrived at the surface of the lenslet. This position was recorded as P1, which is also called the Cat's eye position [31–33], as shown in Figure 8A. Second, the system was switched to the MZI mode. The 3D microlens array was moved along the +*X* direction until the focal plane of the objective lens overlaps with that of the lenslet. This position was recorded as P2, which is called confocal position, as shown in Figure 8B. The distance between P1 and P2 was the back focal length of the lenslet. There were three lenslets measured by using this method. The first lenslet was at the center of the 3D microlens array, with a 5.713 mm focal length. The second lenslet was located between the center and the edge, with a 5.654 mm focal length. The third lenslet was at the edge of the lenslet, with a 5.618 mm focal length. Compared with the nominal back focal length of 5.8 mm, the measured focal lengths were 1.5%, 2.52%, and 3.14% shorter, respectively, due to volume shrinkage during cooling.

In the following section, the OPD, PSF, and MTF of the individual microlens were measured by using the MZI and Intelliwave software (Engineering Synthesis Design, Inc., Tucson, AZ, USA). At first, the optical aberrations caused by the refraction index variation and shape deviation were measured using the MZI, and Figure 9 shows the OPD map of some of the measured lenslets. There were eight lenslets tested, shown in Table 5. Numbers 1 and 2 represent the lenslets at the center part of the 3D microlens array; numbers 3 to 5 are the lenslets at the middle parts; and numbers 6 to 8 are the lenslets close to the edge. From Table 5, we can see that the OPD PV values for lenslets 1 and 2 are less than 0.1350 waves, and the same values are less than 0.1541 waves for lenslets 3 to 5. The PV values increase slightly for lenslets 6 to 8, but still within 1/4 wave. The standard deviation (STD) values for these parameters were calculated and are displayed in the last row in Table 5, indicating that optical performance of the lenslets is homogeneous. The measurements demonstrated that the individual lenslets are very close to the diffraction limit, and of good imaging quality. Optical performance was influenced by geometrical dimension

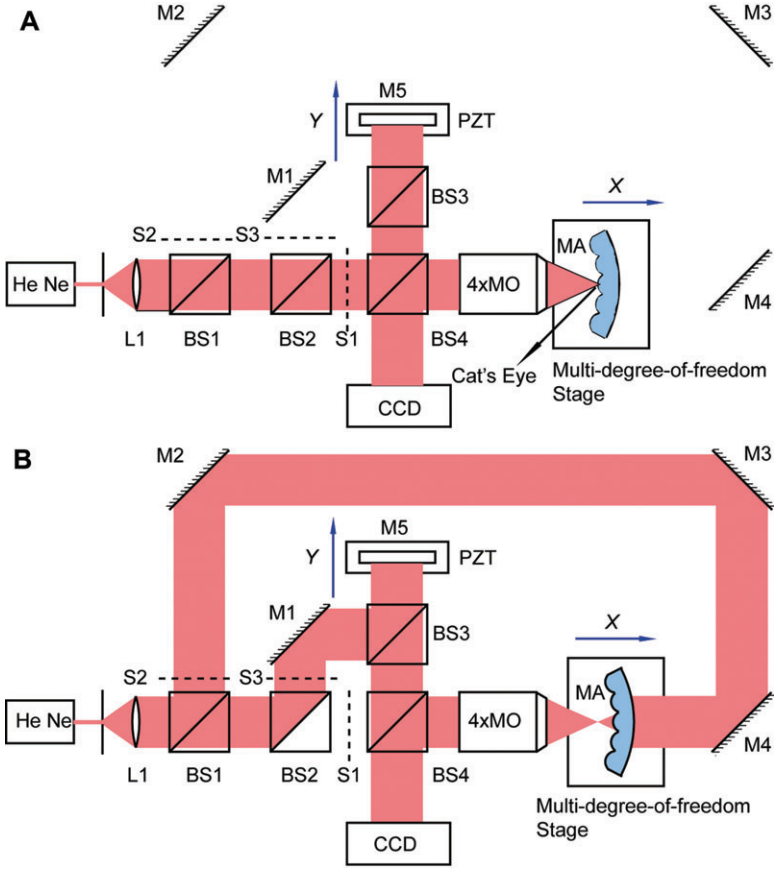

Figure 8 Schematic of the combined interferometers setup: (A) TGI mode; (B) MZI mode.

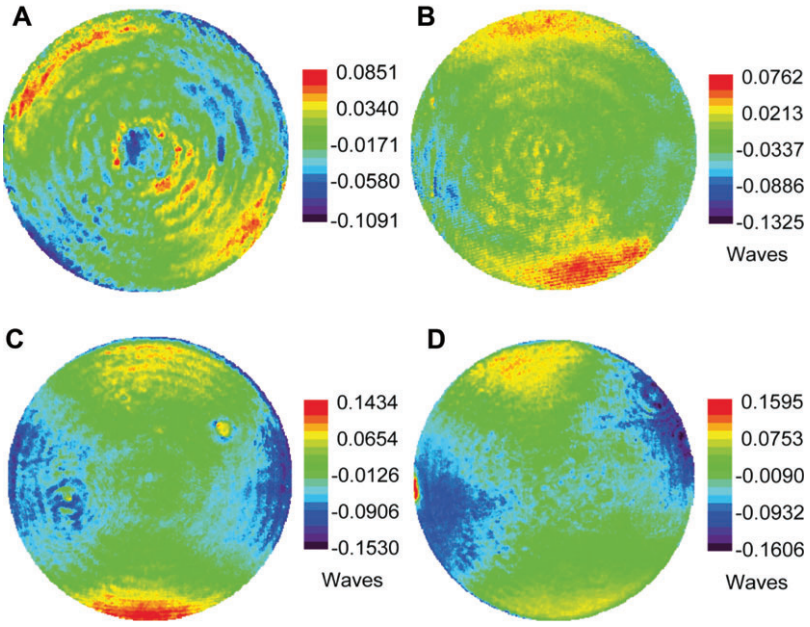

Figure 9 OPD of the lenslets at different locations of the 3D microlens array. (A) OPD of the lenslet at the center; (B) OPD of the lenslet in the middle; (C, D) OPD of lenslets close to the edge.

and index variation. Although the 3D microlens array has volume shrinkage due to the inherent disadvantage of injection molding, the geometrical errors did not dramatically influence the optical performance of individual lenslets. Besides, the index variation was well controlled during the injection molding process.

The PSF of the lenslet was measured using the MZI. As shown in Figure 10A, three diffraction rings can be observed, and the radius of the first dark ring is 19.13 μm with 83% of the energy concentrated at the center, indicating good imaging quality of the lenslet under investigation.

The MTF of the aforementioned three lenslets with known focal lengths was also measured using the MZI. Figure 10B shows the comparison between the ZEMAX simulation and the experiment results. At the given working wavelength 632.8 nm, the frequency cut-off for ZEMAX simulation is 129.06 Lp/mm, whereas the frequency cut-off for the three lenslets is 147.21, 144.10, and 144.02 Lp/mm, separately. The deviation of the frequency cut-off is caused by the difference between the focal lengths.

6 Overall performance of the 3D microlens array in large FOV imaging application

To study the overall performance of the 3D microlens array, an imaging test was conducted using a home-built

Table 5 Optical aberrations for different lenslets.

#	PV98.00% (wave)	RMS (wave)	X Astig (wave)	Y Astig (wave)	X Coma (wave)	Y Coma (wave)	Spherical (wave)
1	0.1322	0.0280	−0.0019	0.0490	−0.0040	−0.0067	−0.0072
2	0.0983	0.0197	−0.0162	0.0301	0.0004	0.0028	−0.0032
3	0.1141	0.0228	−0.0426	0.0098	0.0019	0.0011	0.0021
4	0.1541	0.0308	−0.0638	0.0045	−0.0016	0.0054	−0.0113
5	0.1411	0.0306	−0.0651	-0.0047	−0.0070	0.0135	−0.0038
6	0.2202	0.0437	−0.0941	-0.0025	−0.0146	0.0318	−0.0091
7	0.2146	0.0429	−0.0851	-0.0108	−0.0100	0.0120	−0.0178
8	0.2121	0.0339	0.0144	-0.0060	0.0151	0.0187	−0.0434
STD	0.0484	0.0086	0.0396	0.0207	0.0090	0.0119	0.0134

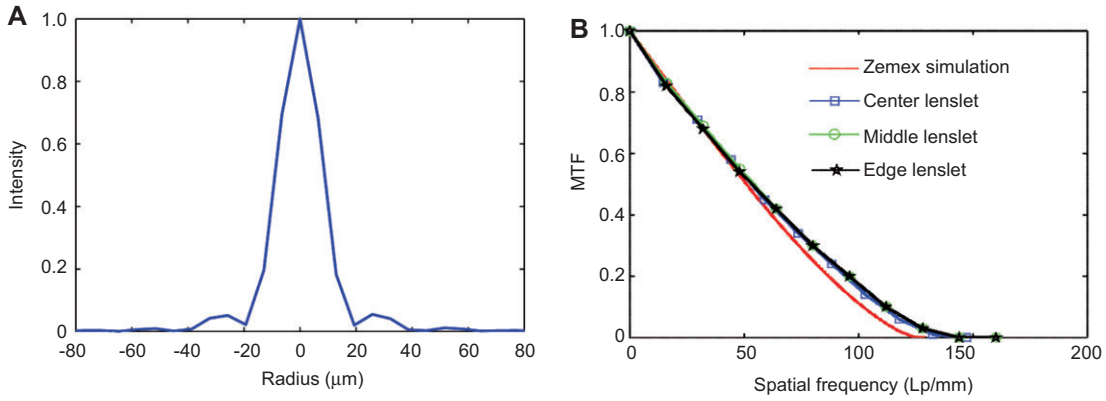

Figure 10 (A) PSF of an individual lenslet. (B) Comparison between the MTFs of three lenslets in ZEMAX simulation. Wavelength = 632.8 nm.

setup as shown in Figure 11A. A computer screen was placed in front of the 3D microlens array. The dimension of the screen is 304 mm × 189 mm. There are three letters, 'O', 'S', and 'U' on the screen function as the targets, each letter has a dimension of 5 mm × 10 mm. The distance between the letter 'O' and the letter 'U' is 299 mm, and the distance L from the screen to the 3D microlens array is 120 mm, which guarantees the screen covers the nominal FOV of the 3D microlens array. This screen was observed from three different directions as illustrated in Figure 11A. First, the screen was observed from the direction of view 1, and Figure 12A is the corresponding image captured in this direction. Figure 12B is the image captured from the direction of view 2, which is parallel to the horizontal line. Figure 12C is the corresponding image captured from the direction of view 3.

Figure 12 shows that every letter was imaged by multiple layers of lenslets, proving the FOV overlap among the adjacent imaging channels. The FOV overlap compensates for the flux limitation caused by the small sizes of the individual lenslet, which is useful for multichannel signal processing. Therefore, the 3D microlens array can be employed for 3D imaging or super-resolution imaging application. The FOV is controllable according to different demands by adding an aperture array in future study. By contrast, Figure 12 also displays the entire screen captured using the 3D microlens array. Restricted by the size of the CCD imager, only images for the lenslets of limited layers were captured every time. For example, there are more than ten layers of lenslets imaging 'S' from the direction of view 2. Considering this limitation, the overall FOV of this 3D microlens array is more than 104°. Figure 12B shows that the imaged 'S' becomes increasingly blurred from the center to the edge. Owing to the position differences and the axis direction variation, the imaging planes of the lenslets are not coincident. To overcome this problem, a device, such as a freeform lens developed in [34] can be employed to transfer the images of different lenslets onto the same planar detector.

7 Future work

In one of the follow-up studies, 3D microlens array will be applied to 3D projection to generate micro features

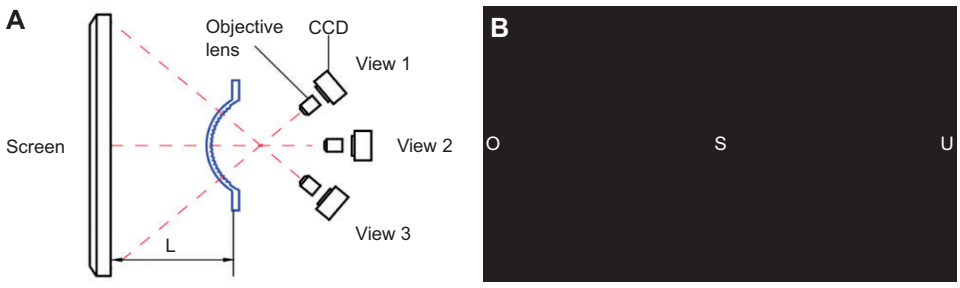

Figure 11 (A) Setup for optical performance test. (B) Screen image of the notebook.

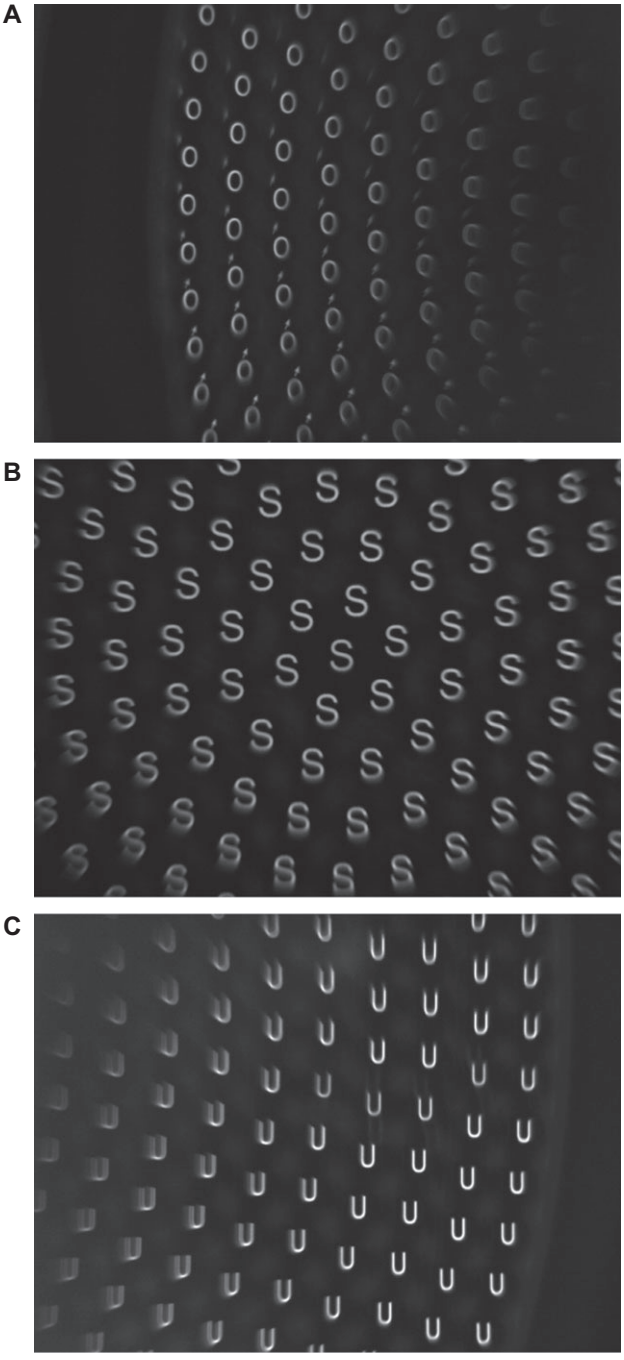

Figure 12 Images of different views: (A) image captured from view 1, (B) image captured from view 2, (C) image captured from view 3.

with higher fill factor on curved substrates. Success of this application will dramatically improve the 3D projection micromachining capability. In other studies, optical devices will be developed based on this 3D microlens array with wide FOV and high fill factor. The technical challenge is the fact that the focal planes of the lenslets distribute on a spherical surface, while most imaging detectors are planar. To overcome this conflict, we are working on an optical device that can transfer the images onto the planar imaging detector. The design of this device was completed and the fabrication is ongoing. The success of this device will be critical to applications such as motion detection and integrated imaging, bringing profound changes to medical and biomedical imaging applications.

8 Conclusion

In this study, a low cost manufacturing process for a precision 3D microlens array on curved substrates was developed using the microinjection molding process and high precision molds machined using the FTS technique. This 3D microlens array has more than 104° overall FOV. Although the lens array has a compact size, it still contains 1219 lenslets evenly distributed on its bottom surface, resulting in a high fill factor. To identify the proper injection molding conditions, different process conditions were experimentally evaluated with the assistance of numerical simulation for best molding results. Specifically, polymer melt temperature, packing pressure, cooling time and mold temperature were determined using numerical simulation to minimize volume shrinkage and the refraction index variation introduced during the injection molding process. More in-depth studies on microinjection molding will be carried out in the future.

The finished 3D microlens array was tested both for geometrical errors and optical performance. The surface roughness was less than 5 nm, the deviation from the designed spherical shape for the individual lenslet was less than 250 nm, and the overall shape deviation from the design value was less than 22 μm. The optical performance of the individual lenslet was evaluated using two different interferometers. The PV values of the OPD were less than 1/4 waves. The OPD, MTF, and PSF of the lens array demonstrated good optical performance of individual lenslets and the feasibility of the manufacturing process. The overall performance of the 3D microlens array was evaluated using a home-built optical test setup. The wide FOV of the 3D microlens array, the FOV overlap among adjacent channels, and the unique imaging capability were verified. In the future, additional components, such as a freeform lens, will be added to transfer the images from different directions into a planar detector for possible imaging applications.

This study illustrated that 3D microlens arrays on curved bases can be fabricated by using the injection molding method to produce high optical quality

components at very low cost. This study also proved that the injection molding process can produce high precision true 3D micro structures in high volume therefore providing a practical solution for many optical applications.

Acknowledgments: This study was partially the result of collaborative efforts between the Ohio State University and Fraunhofer IOF under the Fraunhofer program 'ProfX²'. This study was also based on the work supported by the National Science Foundation under Grant Numbers CMMI-0928521 and EEC-0914790. Any opinions, findings, and conclusions or recommendations expressed in this material are those of the authors and do not necessarily reflect the views of the National Science Foundation. The authors would also like to acknowledge Professional Instruments in Hopkins, MN, USA for their continuous support. The authors acknowledge Donald A. Pearson II and ESDI of Tucson, AZ, USA for the software Intelliwave LE-2 used in this research. The authors would like to acknowledge Likai Li for his assistance in numerical modeling using Moldex 3D software.

Received October 6, 2012; accepted March 3, 2013; previously published online April 2, 2013

References

[1] N. Franceschini, J. M. Pichon and C. Blanes, Phil. Trans. Biol. Sci. 337, 283–294 (1992).
[2] W. C. Goltsos and M. Holz, Optical Eng. 29, 1392–1397 (1990).
[3] J. S. Leggatt and M. C. Hutley, Electron. Lett. 27, 238–240 (1991).
[4] M. Levoy, R. Ng, M. Footer, A. Adams and M. Horowitz, Proc. ACM SIGGRAPH 25, 1–11 (2006).
[5] X. Shen, L. Pan and L. Lin, Sens. Actuat. 97–98, 428–433 (2002).
[6] N. F. Borrelli, D. L. Morse, R. H. Bellman and W. L. Morgan, Appl. Optics 24, 2520–2525 (1985).
[7] D. M. Hartmann, O. Kibar and S. C. Esener, Optical Lett. 25, 975–977 (2000).
[8] E. Roy, B. Voisin, J. F. Gravelb, R. Peytavic, D. Boudreau et al., Microelectron. Eng. 86, 2255–2261 (2009).
[9] J. Tong, C. A. Simmons and Y. Sun, J. Micromech. Microeng. 18, 037004 (2008).
[10] C. Beuret, G. A. Racine, J. Gobet, R. de Luthier and N. F. Rooij, Proc. IEEE Int. Conf. Micro Electro Mechan. Syst. 81–85 (1994).
[11] T. Dillon, M. Zablocki, S. Shi, J. Murakowski and D. Prather, Proc. SPIE 6882, 1–10 (2008).
[12] T. Bourounia, T. Masuzawa and H. Fujita, J. Microelectromech. Syst. 13, 190–199 (2004).
[13] O. Lima, L. Tan, A. Goel, Z. Li and M. Negahban, J. Vacuum Sci. Technol. B 25, 2412–2418 (2007).
[14] H. O. Jacobs, A.R. Tao, A. Schwartz, D. H. Gracias and G. M. Whitesides, Science 296, 323–325 (2002).
[15] D. Zhu, C. Li, X. Zeng and H. Jiang, Appl. Phys. Lett. 16, 081111 (2010).
[16] Y. Zhao, W. Huang and H. Purnawali, Appl. Mechan. Mater. 161, 292–295 (2012).
[17] Y. Zhao, C. Wang, W. Huang, H. Purnawali and L. An, Optics Expr. 19, 26000–26005 (2011).
[18] L. Li, P. He, F. Wang, K. Georgiadis, O. Dambon, et al., J. Optics 13, 055407 (2011).
[19] P. He, F. Wang, L. Li, K. Georgiadis, O. Dambon, et al., Optics 13, 085703 (2011).
[20] A. Y. Yi and L. Li, Optics Lett. 30, 1707–1709 (2005).
[21] L. Li and A. Y. Yi, J. Micromech. Microeng. 19, 105010 (2009).
[22] F. Fang, X. Zhang and X. Hu, Optics Expr. 16, 7323–7329 (2008).
[23] G. E. Davis, J. W. Roblee and A. R. Hedges, Proc. SPIE 7426, 742605 (2009).
[24] S. Scheiding, A. Y. Yi, A. Gebhardt, L. Li, S. Risse, et al., Optical Expr. 19, 23938–23951 (2011).
[25] H. Zhang, L. Li, D. McCray, D. Yao and A.Y. Yi, Sens. Actuat. A Phys. 179, 242–250 (2012).
[26] C. Yang, L. Su, C. Huang, H. Huang, J. Castro, A. Y. Yi, Adv. Polym. Technol. 30, 51–61 (2011).
[27] L. Li, C. Yang, H. Shi, W. Liao, H. Huang, et al., Polym. Eng. Sci. 50, 1594–1604 (2010).
[28] B. K. Lee, D. S. Kim and T. H. Kwon, Microsyst. Technol. 10, 531–535 (2004).
[29] L. S. Turng, M. Peic and D. K. Bradley, J. Inject. Mold. Technol. 6, 143–155 (2002).
[30] T. Maruyama, Y. Noro and M. Muranaka, Kobunshi Ronbunshu 45, 625–632 (1988).
[31] O. Falkenstörfer and J. Schwider, Optical Eng. 34, 2972–2975 (1995).
[32] J. Schwider and H. Sickinger, Optik (Stuttg.) 107, 26–34 (1997).
[33] H. Sickinger, J. Schwider and B. Manzke, Optik (Stuttg.) 110, 239–243 (1999).
[34] L. Li and A. Y. Yi, J. Optics Soc. Am. 27, 2613–2620 (2010).